molecular pharmaceutics

The University of Winnipeg | Library

Subscriber access provided by University of Winnipeg Library

Article

Interplay of Efflux Transporters with Glucuronidation and Its Impact on Subcellular Aglycone and Glucuronide Disposition: A Case Study with Kaempferol

Yuhuan Li, Linlin Lu, Liping Wang, Wei Qu, Wenqin Liu, Yushan Xie, Hongming Zheng, Ying Wang, Xiaoxiao Qi, Ming Hu, Lijun Zhu, and Zhongqiu Liu

Mol. Pharmaceutics, **Just Accepted Manuscript** • DOI: 10.1021/acs.molpharmaceut.8b00782 • Publication Date (Web): 30 Oct 2018

Downloaded from http://pubs.acs.org on October 31, 2018

Just Accepted

"Just Accepted" manuscripts have been peer-reviewed and accepted for publication. They are posted online prior to technical editing, formatting for publication and author proofing. The American Chemical Society provides "Just Accepted" as a service to the research community to expedite the dissemination of scientific material as soon as possible after acceptance. "Just Accepted" manuscripts appear in full in PDF format accompanied by an HTML abstract. "Just Accepted" manuscripts have been fully peer reviewed, but should not be considered the official version of record. They are citable by the Digital Object Identifier (DOI®). "Just Accepted" is an optional service offered to authors. Therefore, the "Just Accepted" Web site may not include all articles that will be published in the journal. After a manuscript is technically edited and formatted, it will be removed from the "Just Accepted" Web site and published as an ASAP article. Note that technical editing may introduce minor changes to the manuscript text and/or graphics which could affect content, and all legal disclaimers and ethical guidelines that apply to the journal pertain. ACS cannot be held responsible for errors or consequences arising from the use of information contained in these "Just Accepted" manuscripts.

ACS Publications

is published by the American Chemical Society. 1155 Sixteenth Street N.W., Washington, DC 20036

Published by American Chemical Society. Copyright © American Chemical Society. However, no copyright claim is made to original U.S. Government works, or works produced by employees of any Commonwealth realm Crown government in the course of their duties.

	University of Science and Technology

SCHOLARONE™
Manuscripts

Title Page

Interplay of Efflux Transporters with Glucuronidation and Its Impact on Subcellular Aglycone and Glucuronide Disposition: A Case Study with Kaempferol

Yuhuan Li[1#], Linlin Lu[1, 2#], Liping Wang[1], Wei Qu[1], Wenqin Liu[1, 4], Yushan Xie[1], Hongming Zheng[1], Ying Wang[1], Xiaoxiao Qi[1], Ming Hu[1, 3*], Lijun Zhu[1*], Zhongqiu Liu[1, 2*]

[1]Joint Laboratory for Translational Cancer Research of Chinese Medicine of the Ministry of Education of the People's Republic of China, International Institute for Translational Chinese Medicine, Guangzhou University of Chinese Medicine, Guangzhou, Guangdong, 510006, PR China.

[2]State Key Laboratory of Quality Research in Chinese Medicine, Macau University of Science and Technology, Macau (SAR), 999078, PR China.

[3]Department of Pharmacological and Pharmaceutical Sciences, College of Pharmacy, University of Houston, Houston, TX 77030, USA.

[4]Department of Pharmaceutics, School of Pharmaceutical Sciences, Southern Medical University, Guangzhou, Guangdong, China.

[#] Authors equally contributed to the paper.

[*] **Corresponding authors:**

Prof. Zhongqiu Liu, Joint Laboratory for Translational Cancer Research of Chinese Medicine of the Ministry of Education of the People's Republic of China, International Institute for Translational Chinese Medicine, Guangzhou University of Chinese Medicine, Guangzhou, Guangdong, 510006, PR China. State Key Laboratory of Quality Research in Chinese Medicine, Macau University of Science and

Technology, Macau (SAR), 999078, PR China. Tel: +8620-39358061; Fax: +8620-39358071; E-mail: liuzq@gzucm.edu.cn.

Dr. Lijun Zhu, Joint Laboratory for Translational Cancer Research of Chinese Medicine of the Ministry of Education of the People's Republic of China, International Institute for Translational Chinese Medicine, Guangzhou University of Chinese Medicine, Guangzhou, Guangdong, 510006, PR China. Tel: +8620-39358401; Fax: +8620-39358071; E-mail: zhulijun@gzucm.edu.cn.

Prof. Ming Hu, Department of Pharmacological and Pharmaceutical Science, College of Pharmacy, University of Houston, Houston, Texas 77030; Tel: 713-795-8302; Fax: 713-795-8305; E-mail: mhu@uh.edu.

Abstract

Glucuronidation is a major process of drug metabolism and elimination that generally governs drug efficacy and toxicity. Publications have demonstrated that efflux transporters control intracellular glucuronidation metabolism. However, it is still unclear whether and how efflux transporters interact with UDP-glucuronosyltransferases (UGTs) in subcellular organelles. In this study, kaempferol, a model fluorescent flavonoid, was used to investigate the interplay of glucuronidation with transport at the subcellular level. Human recombinant UGTs and microsomes were utilized to characterize the *in vitro* glucuronidation kinetics of kaempferol. The inhibition of UGTs and efflux transporters on the subcellular disposition of kaempferol were determined visually and quantitatively in Caco-2/TC7 cells. The knockout of transporters on the subcellular accumulation of kaempferol in liver and intestine were evaluated visually. ROS and Nrf2 were assayed to evaluate the pharmacological activities of kaempferol. The results showed that UGT1A9 is the primary enzyme responsible for kaempferol glucuronidation. Visual and quantitative data showed that the UGT1A9 inhibitor carvacrol caused a significant rise in subcellular aglycone and reduction in subcellular glucuronides of kaempferol. The inhibition and knockout of transporters, such as P-glycoprotein (P-gp), breast cancer resistance protein (BCRP), and multidrug resistance-associated proteins (MRPs), exhibited a marked increase in subcellular kaempferol and decrease in its subcellular glucuronides. Correspondingly, inhibition of UGT1A9 and transporters led to increased kaempferol and, consequently, a significantly enhanced ROS scavenging efficiency and nuclear translocation of Nrf2. In conclusion, the interplay of efflux transporters (P-gp, BCRP and MRPs) and UGTs govern the subcellular exposure and corresponding pharmacological activity of kaempferol.

Keywords

Glucuronidation; UDP-glucuronosyltransferases; efflux transporters; organelles; subcellular distribution; kaempferol; ROS; Nrf2

Abbreviations

BCRP, breast cancer resistance protein; ER, endoplasmic reticulum; HIMs, human intestinal microsomes; HLMs, human liver microsomes; K-3-G, kaempferol-3-glucuronide; K-7-G, kaempferol-7-glucuronide; LSCM, laser scanning confocal microscope; Mito, mitochondria; MRPs, multidrug resistance-associated proteins; NAC, N-acetyl-L-cysteine; Nrf2, nuclear factor E2-related factor 2; P-gp, P-glycoprotein; ROS, reactive oxygen species; UGTs, UDP-glucuronosyltransferases; UHPLC-MS/MS, ultra high performance liquid chromatograpy-tandem mass spectrometry.

Introduction

Glucuronidation, which is catalyzed by UDP-glucuronosyltransferases (UGTs), is one of the most important detoxification pathway in mammals. In humans, glucuronidation is responsible for the elimination of a variety of substances, including endogenous substances (e.g., bile acid), drugs (e.g., SN-38, raloxifene), and dietary phytochemicals, such as polyphenols (e.g., resveratrol, genistein) and flavonoids (e.g., kaempferol, acacetin), and is estimated to account for approximately 35% of phase II metabolism [1]. It has been reported that 15% of the top 200 prescribed drugs in the USA are eliminated directly by glucuronidation [2]. Extensive glucuronidation *in vivo* is a major cause of low bioavailability of various phytochemicals and drugs. The oral bioavailability of flavonoids and coumarins is less than 7% [2,3]. The drug raloxifene, commonly used to treat osteoporosis, has low bioavailability due to extensive glucuronidation [4].

The glucuronidation reaction process attaches a glucuronic acid component to a substrate to generate a glucuronide [5]. Glucuronides are highly polar/hydrophilic molecules that cannot traverse the cell membrane via passive permeation. Human efflux transporters, such as P-glycoprotein (P-gp), breast cancer resistance protein (BCRP), and multidrug resistance-associated proteins (MRPs), are involved in membrane active transport of drugs, xenobiotics, and endogenous substances [6]. BCRP and MRPs have been shown to act as a "Revolving Door" to facilitate and/or control cellular glucuronide excretion [7,8]. Thus, the modification of transporters plays important roles in the pharmacology and toxicology of drugs as well as the endogenous physiology. Generally, many drugs need to enter specific subcellular organelles to reach their targets such as DNA in nuclei; lipophilic peptides or oligoguanidinium in mitochondria, and thus exert their therapeutic effect [9]. UGTs are mainly localized on the luminal side of the endoplasmic reticulum, and also express in other subcellular compartments such as plasma membrane [10], and nuclear membrane [11]. Efflux transporters not only expressed at the plasma membrane, but also at the nuclei [12], mitochondria [13], endoplasmic reticulum [14], lysosome [15], and Golgi apparati [14]. Research have shown that efflux transporters and metabolic enzymes are the key determinants that regulate subcellular distribution of drugs and the concentrations around the binding site as well as the corresponding drug efficacy [16]. For example,

20(S)-ginsenoside Rh2 increased the concentration of adriamycin into its target nuclei by inhibiting P-gp activity, thereby augmenting adriamycin-induced apoptosis [9].

Glucuronidation may be a rate-limiting step in the elimination of xenobiotics and endobiotics. The inhibition of UGTs can increase the blood concentrations of a substrates *in vivo*, whereas the induction of UGT genes would cause a decrease blood concentration of its substrate [9,10]. As an example, morphine-3-glucuronide is significantly enhanced by upregulating UGT2B1 in nonalcoholic steatohepatitis rats [17]. Since the excretion of glucuronides requires the aid of efflux transporters, efflux transports are also a rate-limiting step in controlling the glucuronidation efficiency *in vivo* [18,19]. Recently, a large number of researches have demonstrated that efflux transporters also play a pivotal role in modulating the glucuronidation rate of drugs, ultimately affecting the efficacy/toxicity of drugs [6,17]. For instance, the glucuronidation disposition of thienorphine, a novel opioid agonist, is significantly suppressed by inhibiting P-gp and MRP2 *in vivo* [19].

Because of the coordinated action of glucuronidation by UGTs and efflux by transporters, it is widely accepted that the coupling of UGTs and efflux transporters plays a crucial role in modulating drug glucuronidation [1]. In addition, the transporter function shows great potential in altering glucuronidation [5,14]. For example, cellular glucuronidation of genistein and apigenin is markedly suppressed by the knock-down of MRPs [18]. The interdependence of glucuronidation metabolism and transport is termed “metabolism-transport interplay” and has been demonstrated in cells in different laboratories [1,20,21]. However, whether and how UGTs interact with efflux transporters at the subcellular level remain unclear. A further understanding of the glucuronidation metabolism-transport interplay is of great significance for accurate prediction of drug glucuronidation and its efficacy/toxicity *in vivo*.

This study aims to explore the interplay of glucuronidation with transport at the subcellular level. Kaempferol was used as a model compound because of its autofluorescence and glucuronidation [22,23]. First, we characterized kaempferol glucuronidation using twelve commercially recombinant human UGT isoforms and human intestinal microsomes (HIMs). Laser scanning confocal microscopy (LSCM) and UHPLC-MS/MS were used to analyse the impact of efflux transporters on subcellular glucuronidation based on chemical inhibition and gene knockout experiments. In parallel, we demonstrated that UGT and transporters controlling the

subcellular distribution of kaempferol would affect its pharmacological effect.

Experimental Section

Chemicals and Reagents

Kaempferol, genistein (internal standard, IS), kaempferol-3-glucuronide (K-3-G), and kaempferol-7-glucuronide (K-7-G) were obtained as described previously [23]. Recombinant human UGT isoforms, HIMs and pooled human liver microsomes (HLMs) were purchased from BD Biosciences (Woburn, MA, USA). Uridine diphosphate glucuronic acid (UDPGA), alamethicin, D-saccharic-1,4-lactone, magnesium chloride ($MgCl_2$), carvacrol, Ko143, verapamil, MK571, Hanks' balanced salt solution (HBSS), and the Endoplasmic Reticulum Isolation Kit and Lysosome Isolation Kit were acquired from Sigma-Aldrich (St. Louis, MO, USA). The Mitochondria Fractionation Kit (for isolation of cytosolic & mitochondrial fractions) and Nuclear Extract Kit were acquired from Active Motif (Carlsbad, CA, North America). The 4-6-diamidino-2-phenylindole (DAPI, used as a nuclear stain), MitoTracker® Red CMXRos (used as a mitochondrial stain), ER-Tracker™ Red dye (used as a endoplasmic reticulum stain) and LysoTracker® Red DND-99 (used as a lysosomal stain) were purchased from Thermo Fisher Scientific (MA, USA). The rabbit anti-Nrf2 was obtained from Abcam (Cambridge, MA, USA). All other reagents and solvents were commercially available and of analytical grade.

Cell Culture

Human colon adenocarcinoma cell line Caco-2/TC7 was a kind gift of Dr. Ming Hu (University of Houston, Texas, USA), and cultured in Dulbecco's Modified Eagle's Medium (DMEM) containing 10% fetal bovine serum (FBS), 100 $U \cdot mL^{-1}$ penicillin and 100 $\mu g \cdot mL^{-1}$ streptomycin at 37 °C with 5% CO_2. The cells were passaged every 3-4 days (at 80% confluence). Caco-2/TC7 cells at passage 48-69 were used for the experiments.

Animals

8-week-old male wild-type FVB mice were obtained from Vital River Laboratory Animal Technology Co., Ltd. (Beijing, China). Male $Mdr1a^{-/-}$, $Bcrp1^{-/-}$ and $Mrp2^{-/-}$ mice (aged 8 weeks) with a FVB genetic background were purchased from Biomodel Organism Science & Technology Development Co., Ltd. (Shanghai, China). The efflux transporter knockout FVB mice were identified by the Sanger sequencing method (Chain Termination Method). All mice were housed for at least one week

under ambient controll conditions (temperature 23 ± 2 °C, humidity 55% ± 5%, and 12 hour light/dark cycle) prior to the experiment. The animal experiments used in this assay were approved by Ethics Committee of Guangzhou University of Chinese Medicine (No. 014449430106). Mice were fasted overnight and free to drink water before the experiment.

UHPLC–MS/MS Conditions

Agilent 1290 series UHPLC

The UHPLC conditions were: Zorbax C_{18} column (100 × 3.0 mm, 1.8 μm, Agilent Technologies); mobile phase A, 0.05% formic acid aqueous solution; mobile phase B, acetonitrile; gradient, 0 – 4.5 min, 23% B; 4.5 – 5.0 min, 53%B; 5.0 – 8.0 min, 23% B; injection volume, 5 μL; and flow rate, 0.4 $mL \cdot min^{-1}$.

Agilent 6490 Triple Quadrupole mass spectrometer

The mass spectrometer was equipped with an electrospray ionization source. Kaempferol and its glucuronides (K-3-G, K-7-G) were quantified by using multiple reaction monitoring (MRM) scan type in negative mode The parameters were set as follows: capillary voltage, 3.5 KV; nozzle voltage, 1000 V; gas temperature, 290 °C; sheath temperature, 340 °C; fragmentation voltages, 380 V, delta electron multiplier voltage, 200 V. Quantification was performed using transitions of m/z 461.0→285.0 (187.0 qualifier) for K-3-G and K-7-G; m/z 285.0→93.0 (187.0 qualifier) for kaempferol; and m/z 269.0→132.9 for IS.

Glucuronidation Assay

Glucuronidation rates of kaempferol by twelve recombinant human UGTs were determined at three concentrations (1.25, 2.5 and 10 μM). The glucurono-incubation system was performed according to a previous study [3]. In brief, UGT Supersomes™ (0.0106 $mg \cdot mL^{-1}$) were mixed with UDPGA (3.5 mM), $MgCl_2$ (0.88 mM), saccharolactone (4.4 mM), alamethicin (0.022 $mg \cdot mL^{-1}$), and kaempferol in a 50 mM potassium phosphate buffer. The mixtures (100 μL) was incubated at 37 °C for 20 min. After incubation, 50 μL of methanol containing 200 nM IS was added to the mixture, and then vortexed immediately. Following by centrifuging at 19357 g for 25 min, a volume of 5 μL of the supernatant was injected for UHPLC-MS/MS analysis.

To estimate kinetic parameters, serial concentrations of kaempferol (0.125-40.0 μM)

were incubated with UGT1A9, HIMs and HLMs at 37 ℃ for 20 min. The final protein concentrations were 0.0625-0.200 mg·mL^{-1} and other detailed procedures are described above. Kinetic parameters were then analyzed according to the profile of Eadie-Hofstee plots as described previously [24,25]. The goodness of fit was evaluated based on R^2 values and Akaike's information criterion.

Subcellular Distribution of Kaempferol in Live Cells

Caco-2/TC7 cells were seeded at 5.0 × 10^4 cells /well in a 35-mm glass bottom dish. When the cells reached ~70% confluency, the complete DMEM was removed from the culture dish, and the cells were rinsed three times with prewarmed HBSS (PH = 7.4). The cells were then treated with HBSS solution containing kaempferol (50 μM) with or without UGT1A9 and efflux transporter inhibitors for 5, 15, 30, 45, 60 min in the dark at 37 °C. We used the working concentrations of 100 μM for UGT1A9 inhibitor carvacrol, 10 μM for BCRP inhibitor Ko143, 50 μM for P-gp inhibitor verapamil and 50 μM for MRPs inhibitor MK571.

After incubation, the cells were rinsed three times with prewarmed PBS, followed by staining with various organelle-specific fluorescent dyes. Nuclei were fixed for 20 min with 4% paraformaldehyde and then stained with 2 μg·mL^{-1} DAPI for 20 min, mitochondria were stained with 300 nM MitoTracker® Red CMXRos for 40 min, endoplasmic reticulum was stained with 500 nM ER-Tracker™ Red dye for 30 min and lysosome was stained with 75 nM Lyso Tracker® Red DND-99 for 80 min. Images of Caco-2/TC7 cells were collected by laser scanning confocal microscopy (LSCM, Leica-Microsystems, TCS SP8) with a 63 × 1.4 oil-immersion objective with identical settings. The fluorescence of kaempferol (green), DAPI (blue), MitoTracker® Red CMXRos (red), ER-Tracker™ Red dye (red) or Lyso Tracker® Red DND-99 (red) was excited and collected at 488/497-593, 405/413-470, 552/604-733, 552/585-695 or 552/585-695 nm, respectively. To quantify the data, images were analyzed using Image-Pro Plus 6.0. Fluorescence densities of kaempferol after background subtraction were interpreted as quantitative measurements.

To investigate kaempferol dynamics, time-lapse analyses were performed using a LSCM with a 63 × 1.4 oil-immersion objective. The nuclei and mitochondria were stained with Hoechst 33342 (0.5 μg·mL^{-1}) and MitoTracker® Red CMXRos (450 nM) for 20 min at 37 °C. After staining, the cells were rinsed three times with prewarmed

HBSS, followed by loading with 100 μM of kaempferol with or without chemical inhibitors. Then, a glass bottom dish was placed in a temperature-controlled chamber set to 37 °C equipped with a humidifier set to 90%. Images were acquired ever 30 s with an exposure time of 45 min for all experiments in this work.

Absolute Quantification of Kaempferol and Its Glucuronides in Subcellular Organelles

Caco-2/TC7 cells were cultured in 75 cm^2 flasks. When reached ~90% confluency, cells were treated as in the subcellular distribution assay. However, the working concentration of kaempferol was 20 μM. After incubation, the kaempferol solution was removed, and the cells were washed three times with cold PBS. The nuclei, mitochondria, cytosol, endoplasmic reticulum and lysosomal fractions were isolated using the Nuclear/Mitochondria/Endoplasmic reticulum/Lysosome Isolation Kit. The protein contents of each fraction were measured using the BCA protein assay kit (Bio-Rad, Beyotime, China).

Subcellular samples were prepared as follows: 40 μL of the samples, 10 μL of blank methanol and 50 μL of methanol containing 200 nM genistein were mixed and then vigorously vortexed for 2 min. Calibration standards were prepared as follows: 40 μL of blank cell lysates, 10 μL of working solutions and 50 μL of methanol containing 200 nM genistein were mixed and then vigorously vortexed for 2 min. After centrifugation at 19357 g for 30 min, 5 μL of supernatant was injected into the UHPLC–MS/MS system for quantitative analysis and then normalized to the protein amounts.

Knockout of Efflux Transporters on the Subcellular Accumulation of Kaempferol in Liver and Intestine

Kaempferol suspensions were prepared with 25% (w/v) hydroxypropyl β-cyclodextrin aqueous solution. Wild-type and transporter knockout FVB mice were orally administrated with 100 $mg \cdot kg^{-1}$ kaempferol. After 30 min of treatment, mice were sacrificed by cervical dislocation, and liver and jejunum were rapidly removed. The tissues were rinsed with ice cold saline. After being cut into 1 mm × 1 mm pieces, the tissues were embedded in a tissue freezing medium (Leica) and cut with a cryostat microtome into sections of 4 μm. The tissue sections were mounted on microslides and fixed in acetone for 10 min. After washing with saline, the tissue were stained with

DAPI (5 μg·mL^{-1}) and MitoTracker® Red CMXRos (450 nM) simultaneously for 20 min at 25 °C. After staining, the tissue were rinsed three times with saline and observed with a LSCM.

Detection of Intracellular ROS

The Caco-2/TC7 cells were cultured in a 35-mm glass bottom dish (5.0×10^4 cells /well) for 48 h at 37 °C. Then, the cells were exposed to kaempferol (20 and 50 μM) in the absence or presence of chemical inhibitors for 30 min. The working concentrations were 100 μM for carvacrol, 10 μM for Ko143, 50 μM for verapamil and 50 μM for MK571. N-acetyl-L-cysteine (NAC, 5 mM) was used as a positive control to demonstrate the reduction ofROS. After treatment, the intracellular ROS was labelled with CellROX® Orange Reagent (5 μM), and the nuclei was stained with Hoechst 33342 (1 μg·mL^{-1}). Images were obtained using a LSCM, and fluorescence densities of ROS were measured with Image-Pro Plus 6.0 software.

Immunofluorescence for Nrf2

The Caco-2/TC7 cells were were cultured and treated the same as above section (detection of Intracellular ROS). After treatment, the cells were fixed in 4% formaldehyde (20 min), permeabilized with 0.5% Triton X-100 for 20 min and then incubated in 2% bovine serum albumin in PBS for 1 h. They were then incubated with the primary antibody (rabbit anti-Nrf2, 1:200) overnight at 4 °C. The secondary antibody, goat anti-rabbit IgG H&L (Alexa Fluor® 594), was used at 2 μg·mL^{-1} for 1 h. Nuclear DNA was labelled in blue with DAPI (5 μg·mL^{-1}). Immunofluorescence was imaged with a LSCM. Fluorescence densities of Nrf2 were analyzed by Image-Pro Plus 6.0 software.

Data Analysis

Data are expressed as the mean ± standard deviation (SD). Statistical differences were assessed by software SPSS 19.0 using an independent- sample T test . Correlation analyses were conducted using a Pearson product-moment correlation. Differences were considered to be significant at $P < 0.05$.

Results

In Vitro Glucuronidation Characteristics of Kaempferol

Twelve recombinant human UGTs were utilized to identify UGTs involved in the glucuronidation of kaempferol. As showed in Figure 1A, K-3-G formation was catalyzed mainly by UGT1A9, and UGT1A1 and UGT2B7 also generated a small quantity of K-3-G. K-7-G formation was catalyzed mainly by UGT1A9, and UGT1A1 and UGT1A10 and UGT2B7 also generated a small quantity of K-7-G (Figure 1B).

UGT1A9 mediated glucuronidation of kaempferol following classic Michaelis-Menten kinetics, as evidenced by a linear Eadie-Hofstee plot (Figures 1C-1H). The intrinsic clearance (*CL;* V_{max}/K_m) of K-3-G and K-7-G in UGT1A9 were 1071.43 and346.67 $\mu L \cdot min^{-1} \cdot mg^{-1}$, respectively (Figures 1C and 1D). HIMs and HLMs mediated glucuronidation of kaempferol following Biphasic kinetics. The *CL1* and *CL*2 of K-3-G in HIMs were 340, 140 and 10, 90 $\mu L \cdot min^{-1} \cdot mg^{-1}$ in HLMs, respectively (Figures 1E and 1G). The *CL1* and *CL*2 of K-7-G in HIMs were 310, 60 and 60000, 170 $\mu L \cdot min^{-1} \cdot mg^{-1}$ in HLMs, respectively (Figures 1F and 1H).

UGT1A9 and Efflux Transporter Inhibitors Increased the Fluorescence Densities of Kaempferol in Subcellular Organelles

Confocal imaging plus image video analysis was used to monitor the accumulation of kaempferol in subcellular organelles using a staining technique. First, the nuclear accumulation of kaempferol over time was visualized by laser scanning confocal microscopy (LSCM) (Figure 2A, Figures S1A-S1F). The increased green fluorescence was colocalized with blue fluorescence, suggesting that kaempferol was entrapped in nuclei. Next, we visualized the accumulation of kaempferol in mitochondria, endoplasmic reticulum and lysosome at various time points (Figures 2B-2D, Figures S2A-S2F, Figures S3A-S3F, Figures S4A-S4F). The increased green fluorescence was overlapped with red fluorescence, suggesting that kaempferol aggregated in the mitochondria, endoplasmic reticulum, or lysosome. The maximum green fluorescent densities (kaempferol) that accumulated in nuclei (0.06), mitochondria (0.09), endoplasmic reticulum (0.051), or lysosome (0.07) were achieved as early as 30 min. The green fluorescent densities gradually decreased after 30 minutes in the absence or presence of chemical inhibitors. According to the fluorescent quantitative value,

(Figures 2a-2d), the mitochondrial kaempferol were elevated compared with those in the nuclei, endoplasmic reticulum and lysosome.

The UGT1A9 inhibitor carvacrol markedly increased the green fluorescence signal of kaempferol in all subcellular organelles (Figure 2). The effects of single/multiple transporter(s) on the subcellular accumulation of kaempferol were further investigated. The BCRP inhibitor Ko143, P-gp inhibitor verapamil and MRPs inhibitor MK571 substantially enhanced the uptake rate and accumulation of kaempferol in all subcellular organelles, indicating that UGT metabolism of kaempferol was inhibited when the efflux function was inhibited. The fluorescence signal of kaempferol was highest when the three inhibitors were used in combination.

To record time-lapse videos, we used LSCM to achieve a time resolution of 30 s for all experiments in this work. Video S1 recorded the dynamic accumulation of kaempferol in nuclei**.** Video S2 showed the simultaneous recording of nuclear and mitochondrial behavior and kaempferol dynamics. Kaempferol behavior was identical to direct optical observation.

UGT1A9 and Efflux Transporter Inhibitors Caused a Rise of Kaempferol and Reduction of Its Glucuronides in Subcellular Organelles

First, we developed and validated a sensitive UHPLC-MS/MS method to determine the intracellular/subcellular levels of kaempferol and its glucuronides. No endogenous interference was observed in the chromatogram (Figures S5A-S5F). The precision and accuracy of intra-day and inter-day assay showed that the developed method was reliable and had good reproducibility and accuracy (Table S1). The mean recovery values suggested that the method could ensure the acquisition of accurate data. The analytes did not exhibit an obvious matrix effect (Table S2). The results of stability experiments indicated that kaempferol in the cell lysate was stable after being stored at −20 °C for 15 days, at room temperature for 5 h and through three freeze-thaw cycles (Table S3).

After Caco-2/TC7 cells were incubated with 20 μM kaempferol with or without UGT1A9 and efflux transporter inhibitors, the concentrations of kaempferol, K-3-G and K-7-G were determined, and their mean subcellular concentration-time curves are shown in Figure 3. Kaempferol was quickly absorbed in Caco-2/TC7 cells, and considerable amounts of kaempferol could be measured in the cytosol (2.14

nmol·mg^{-1}), mitochondria (0.02 nmol·mg^{-1}), endoplasmic reticulum (0.48 nmol·mg^{-1}), lysosome (0.42 nmol·mg^{-1}) and nuclei (0.45 nmol·mg^{-1}) after incubation for 5 min (Figures 3A-3E). The maximum subcellular concentrations of kaempferol in Caco-2/TC7 cells were achieved as early as 30 min. Notably, the amounts of kaempferol in isolated mitochondria (1.50 nmol·mg^{-1}) were 3-fold higher than those in nuclei/lysosomes (0.57 nmol·mg^{-1}) and 2-fold higher than those in endoplasmic reticulum (0.76 nmol·mg^{-1}) after incubation for 30 min (Figures 3A-3E). Additionally, K-3-G and K-7-G were detected in all subcellular compartments, and K-3-G was the main glucuronide (Figures 3F-3O). The amounts of metabolites were lower than those of kaempferol.

Moreover, the carvacrol was used to confirm UGT isoforms involved in kaempferol glucuronidation metabolism. The results showed that carvacrol markedly increased the levels of kaempferol in all subcellular organelles in a time-dependent manner (Figures 3A-3E). Carvacrol significantly decreased the accumulation of K-3-G and K-7-G in all subcellular compartments (Figures 3F-3O), in agreement with our previous experimental findings shown in Figure 1.

The effects of single/multiple transporter(s) on the subcellular accumulation of kaempferol and its glucuronides were further investigated. The Ko143, verapamil and MK571 markedly elevated the uptake rate and accumulation of kaempferol in all subcellular organelles in a time-dependent manner, respectively. When the three inhibitors were used in combination, the concentrations of kaempferol were highest (Figures 3A-3E). Ko143, verapamil, and MK571 significantly reduced the subcellular concentrations of K-3-G and K-7-G. When the three inhibitors were used in combination, the concentrations of K-G were lowest in all subcellular organelles (Figures 3F-3O). Since the concentration-time curves used only one bottle of cells, triplicate samples were taken for detection. To verify our data, we further repeated the assays for 30 min of Figure 3, in three independent experiments (Figures S6A-S6C) and found similar results.

To estimate subcellular distribution of the kaempferol and its glucuronides, their content in subcellular organelles were calculated and expressed as percentage of sum of all the quantified 5 subcellular fractions. The complete data were plotted in Figure S7. Overall, kaempferol was distributed in the following rank order with or without chemical inhibitor(s): cytosol > mitochondria > endoplasmic reticulum > nuclei >

lysosome (Figures S7A-S7F). In addition, K-3-G and K-7-G were distributed in the following rank order with or without chemical inhibitor(s): cytosol > endoplasmic reticulum > lysosome > nuclei > mitochondria. In the presence of chemical inhibitor(s), the percentage of kaempferol, K-3-G and K-7-G in cytosol all decreased and, in contrast, in other organelles all increased (Figures S7G- S7R).

Correlation of Fluorescence Density with Absolute Amounts

The relative fluorescence densities (from LSCM) of kaempferol were compared with its absolute amounts (from UHPLC-MS/MS). As showed in Figure 4, high correlations between relative fluorescence densities and absolute amounts were observed with correlation coefficient values of more than 0.74 (in particular, correlation coefficient for mitochondria and lysosome were 0.89 and 0.96, respectively).

Knockout of Efflux Transporters Increased the Subcellular Accumulation of Kaempferol in Liver and Intestine

Efflux transporter knockout mice were used to further confirm our results. After oral administration of kaempferol, kaempferol was mainly distributed in the intestine (Figure 5B), followed by the liver (Figure 5A) in both wild-type and efflux transporter knockout FVB mice. The increased green fluorescence was mainly overlapped with red fluorescence, suggesting that kaempferol was mainly entrapped in mitochondria. Kaempferol fluorescence was quantified and showed in Figure 5C. Kaempferol levels were increased in the liver and intestine of transporter knockout mice. The distribution of kaempferol in the liver of Mdr1a$^{-/-}$ (1.63-fold), Bcrp1$^{-/-}$ (2.17-fold) and Mrp2$^{-/-}$ (2.91-fold) mice was higher than that in wild-type mice ($P < 0.001$). In addition, significantly higher levels was observed in the jejunum of Mdr1a$^{-/-}$ (1.49-fold), Bcrp1$^{-/-}$ (2.02-fold) and Mrp2$^{-/-}$ (2.63-fold) mice compared with wild-type mice ($P < 0.01$).

Kaempferol Potentially Suppressed Intracellular ROS Formation

It has been demonstrated that kaempferol is a scavenger of free radicals and superoxide radicals with a potential role in the counteraction of oxidative stress [19,20]. In parallel, we investigated whether UGT and efflux transporters regulating glucuronidation of kaempferol would affect ROS scavenging. As showed in Figure 6A and 6B, kaempferol treatment decreased the fluorescence of intracellular ROS in a

dose-dependent manner. Moreover, the ROS scavenging efficiency of kaempferol was comparable to N-acetyl-L-cysteine (NAC). Kaempferol co-treated with carvacrol, Ko143, verapamil, and MK571 alone or in combination markedly ($P < 0.001$) decreased the levels of ROS. The chemical inhibitor group had no effect on ROS generation.

Kaempferol Potentially Induced the Expression and Nuclear Translocation of Nrf2

Nrf2 is a master transcription factor regulating a wide range of genes for antioxidant enzymes in response to oxidative stress [28,29]. To determine whether kaempferol-reduced ROS was related to the activation of Nrf2, the expression and localization of Nrf2 was studied. As showed in Figure 7A and 7B, kaempferol treatment increased the expression and nuclear translocation of Nrf2 in a dose-dependent manner. When co-treated with chemical inhibitors, the levels of Nrf2 in cytosol and nuclei were apparently increased ($P < 0.001$) in response to an increase in kaempferol concentrations. The chemical inhibitor group had no effect on Nrf2 expression and translocation.

Discussion

In this work, we for the first time provided confocal imaging and time-lapse videos to demonstrate that efflux transporters have modulatory effects on glucuronidation at the subcelluar level. Confocal images showed that the green fluorescence could co-localize with nuclei, mitochondria, endoplasmic reticulum and lysosome, qualitatively confirming that kaempferol was entrapped in these subcellular organelles. The maximum green fluorescent densities (kaempferol) were achieved as early as 30 min, and gradually decreased after 30 minutes in all subcellular organelles. It has been reported that flavonol loses its autofluorescence when a sugar moiety/functional group is bound to the C3-position [22], indicating that the kaempferol was metabolized by UGTs and led to the disappearance of green fluorescence. The UGT1A9 inhibitor carvacrol, BCRP inhibitor Ko143, P-gp inhibitor verapamil and MRPs inhibitor MK571 markedly increased the green fluorescence densities and decreased the rate of fluorescence elimination in subcellular organelles at all time points (Figure 2). These results indicate that inhibition of UGT enzyme and transporters led to significantly reduced glucuronidation (or elevated kaempferol exposure) in subcellular organelles. Moreover, we trace the dynamic accumulation of kaempferol in nuclei and mitochondrial in real time (Videos S1 and S2), and observed identical results.

To quantitatively evaluate the regulatory effect of efflux transporters on glucuronidation, a cell fraction approach was utilized to separate cytosol, mitochondria, nuclei, endoplasmic reticulum and lysosome. The concentrations of kaempferol and its glucuronides were simultaneously measured by UHPLC–MS/MS. The time-concentration curves illustrated that kaempferol was quickly absorbed and metabolized by UGT enzymes in all subcellular organelles. The carvacrol caused a significant rise in subcellular aglycone, namely, the parent compound of kaempferol, and reduction of subcellular glucuronides in a time-dependent manner. Our results are consistent with a previous study in which UGT1A9 is the primary enzyme responsible for the glucuronidation of kaempferol (Figure 1). Our published research [23] has demonstrated that kaempferol mainly undergoes glucuronidation metabolism to K-3-G and K-7-G *in vivo*, of which K-3-G is the main metabolite. BCRP and MRP2 are responsible for the excretion of K-3-G and K-7-G [23]. In this study, single/multiple transporter(s) inhibitors (Ko143, verapamil, and MK571) resulted in marked increases in subcellular aglycone and significant decreases in subcellular glucuronides,

revealing that inhibition of efflux transporters resulted in significant decreases in cellular glucuronidation of flavonoids [17], providing evidence that subcellular glucuronidation depended on efflux transporters.

Intracellular glucuronides usually increase when the efflux transporter function is inhibited [6,30]. It can be explained by the theory of the "Revolving Door" [7,25], which is based on hydrophilic metabolites that depend on the efflux transporter(s) to exit the cells. Since the glucuronides are the substrates of efflux transporters, inhibition of the transporters blocks glucuronide transport, leading to the subcellular accumulation of glucuronides. However, it is noteworthy that the subcellular levels of kaempferol-glucuronides were significantly decreased in this study. It may be related to the hydrolysis of K-3-G and K-7-G to their parent compound (kaempferol) within Caco-2/TC7 cells (Figure S8)when the reverse reaction occurs (e.g., β-glucuronidase is present in enterocytes) [31]. This phenomenon is also in line with our results, in which kaempferol exhibited considerably higher concentrations in subcellular organelles than its glucuronides. In addition, it has been reported that knock-down of the BCRP causes a significant decrease in intracellular levels of genistein glucuronides, and MRP3 silencing results in a marked reduction in intracellular levels of apigenin glucuronides because of hydrolysis reactions [11].

Efflux transporter knockout mice were utilized to further verify the effect of efflux transporters on glucuronidation in subcellular organelles. It is well-accepted that P-gp (Mdr1a), BCRP and MRP2 are localized to apical membranes of liver and intestine [32]. When glucuronides function as the substrates of these transporters, knockout of these transporters can reduce the biliary excretion and intestinal efflux. Suppressed efflux of glucuronides leads to reduced glucuronidation or elevated drug exposure in plasma and tissue [1]. We analyzed visually the subcellular accumulation of kaempferol in the liver and small intestine of wild-type and transporter knockout mice. Nuclei and mitochondria in the tissue were simultaneously labeled with fluorescent probes. Confocal images showed that kaempferol mainly accumulated in the small intestine, followed by the liver (Figure 5), which is in good agreement with the metabolic characteristics (enterohepatic recycling) of kaempferol [23,33]. We found that kaempferol fluorescence in the liver and intestine of Mdr1a$^{-/-}$ (~1.56-fold), Bcrp$^{-/-}$ (~2.10-fold) and Mrp2$^{-/-}$ (~2.77-fold) mice was markedly enhanced in comparison to wild-type mice,

indicating that the deficiency of transporters led to reduced glucuronidation (or elevated aglycone exposure) in subcellular organelles.

We further determined the effects of UGT enzyme and efflux transporters on the pharmacological activities of kaempferol using the same time point and dose as in the subcellular distribution study. Kaempferol-induced ROS formation as well as the expression and localization of Nrf2 were assayed to evaluate its pharmacological effect. Our data demonstrated that the inhibition of UGT and transporters limited glucuronidation, leading to subcellular accumulation of kaempferol, enhancing ROS scavenging efficiency as well as the corresponding expression and nuclear translocation of Nrf2 (Figures 6 and 7). In addition, Zhang et al. showed that inhibition of P-gp activity increased the accumulations of adriamycin in the nuclei, in turn enhancing its cytotoxic effect on MCF-7/Adr cells [34]. These results indicated that efflux transporters and metabolic enzymes are the key determinants governing the intracellular/subcellular distribution of drugs as well as the corresponding drug efficacy [16,35].

This is the first study to confirm that kaempferol predominantly accumulates in mitochondria. Visual images of cells and tissues illustrated that the green fluorescence (kaempferol) was mainly colocalized with mitochondria. Absolute quantitative analysis showed that the concentrations of kaempferol were approximately 2- to 3-fold higher in the mitochondrial fraction than in the nuclear, lysosomal, and endoplasmic reticulum fractions. These findings could help to explain its antioxidant activities. Kaempferol is a radical scavenger [20] and reaches sites of free radical generation, especially when mitochondria are the primary source of ROS [36]. As a useful antioxidant agent, kaempferol plays a potential role in the prevention and treatment of aging and oxidative stress-related diseases, such as osteoporosis [37], atherosclerosis [38], inflammation [20], neurodegenerative disorders [39], and ischemia-reperfusion injury [40].

The fluorescence imaging method and cell fraction approach are complementary to confirm the subcellular distribution of the chemical. Using a LSCM, the subcellular accumulation sites of the compound can be visualized directly based on the characteristic morphology of stained compartments. However, this method is not able to measure absolute concentrations of compound in subcellular fractions and is not feasible for non-fluorescent compounds [41,42]. Using the cell fraction approach, the

subcellular concentration of compound can be quantitatively evaluated. However, it is difficult to evaluate the subcellular localization of the compound in intact cells with these analytical techniques [9,43]. In this study, the relative fluorescence density (from LSCM) and absolute amounts (from UHPLC-MS/MS) of kaempferol showed high correlation coefficients (r^2 = 0.740 - 0.957). The Caco-2/TC7 cell model was chose in this study because kaempferol also exhibited high glucuronidation rates in the intestinal tract [23]. It is also necessary to use other cells, such as Hep-G2 and Hepa-RG to observe this subcellular interplay between UGT1A9 and transporters in further studies.

In conclusion, we systematically demonstrated the interplay of efflux transporters (P-gp, BCRP and MRPs) with glucuronidation and its impact on subcellular aglycone and glucuronide disposition. Efflux transporters and UGT1A9 govern the subcellular distribution of kaempferol and corresponding pharmacological effect. Kaempferol, a radical scavenger, specifically accumulated into the mitochondria, which may play a potential role in against oxidative stress-related inflammatory diseases and aging.

Author Contributions

Y.H.L., L.J.Z., L.L.L., M.H. and Z.Q.L. designed the experiments. Y.H.L., W.Q., Y.S.X., W.Q.L. and H.M.Z. performed the experiments. X.X.Q. and Y.W. contributed new reagents or analytic tools. L.L.L., L.J.Z., M.H. and Z.Q.L. performed data analysis. Y.H.L., L.P.W., L.J.Z., M.H. and Z.Q.L. wrote or contributed to the writing of the manuscript.

Acknowledgments

This work was supported by the projects of National Natural Science Foundation of China [81720108033 and 81603379], Natural Science Foundation of Guangdong Province [2015A030312012 and 2015B020233015], and Guangdong Province Universities and Colleges Pearl River Scholar Funded Scheme (2015 and 2016).

Competing Interests

The authors declare that no competing interests exist.

References

(1) Yang, G.; Ge, S.; Singh, R.; Basu, S.; Shatzer, K.; Zen, M.; Liu, J.; Tu, Y.; Zhang, C.; Wei, J.et al. Glucuronidation: driving factors and their impact on glucuronide disposition. *Drug. Metab. Rev.* **2017**, *49* (2), 105-138.

(2) Wienkers, L. C.; Heath, T. G. Predicting in vivo drug interactions from in vitro drug discovery data. *Nat. Rev. Drug. Discov.* **2005**, *4* (10), 825-833.

(3) Zhu, L.; Lu, L.; Zeng, S.; Luo, F.; Dai, P.; Wu, P.; Wang, Y.; Liu, L.; Hu, M.; Liu, Z. UDP-Glucuronosyltransferases 1A6 and 1A9 are the Major Isozymes Responsible for the 7-O-Glucuronidation of Esculetin and 4-Methylesculetin in Human Liver Microsomes. *Drug. Metab. Dispos.* **2015**, *43* (7), 977-983.

(4) Sun, D.; Jones, N. R.; Manni, A.; Lazarus, P. Characterization of raloxifene glucuronidation: potential role of UGT1A8 genotype on raloxifene metabolism in vivo. *Cancer. Prev. Res. (Phila.)* **2013**, *6* (7), 719-730.

(5) Tukey, R. H.; Strassburg, C. P. Human UDP-glucuronosyltransferases: metabolism, expression, and disease. *Annu. Rev. Pharmacol. Toxicol*. **2000**, *40*, 581-616.

(6) Ge, S.; Gao, S.; Yin, T.; Hu, M. Determination of pharmacokinetics of chrysin and its conjugates in wild-type FVB and Bcrp1 knockout mice using a validated LC-MS/MS method. *J. Agric. Food. Chem.* **2015**, *63* (11), 2902-2910.

(7) Jeong, E. J.; Liu, X.; Jia, X.; Chen, J.; Hu, M. Coupling of conjugating enzymes and efflux transporters: impact on bioavailability and drug interactions. *Curr. Drug. Metab.* **2005**, *6* (5), 455-468.

(8) Wei, Y.; Wu, B.; Jiang, W.; Yin, T.; Jia, X.; Basu, S.; Yang, G.; Hu, M. Revolving door action of breast cancer resistance protein (BCRP) facilitates or controls the efflux of flavone glucuronides from UGT1A9-overexpressing HeLa cells. *Mol. Pharm.* **2013**, *10* (5), 1736-1750.

(9) Zheng, N.; Tsai, H. N.; Zhang, X.; Rosania, G. R. The subcellular distribution of small molecules: from pharmacokinetics to synthetic biology. *Mol. Pharm.* **2011**, *8* (5), 1619-1628.

(10) Ziegler, K.; Tumova, S.; Kerimi, A.; Williamson, G. Cellular asymmetric

catalysis by UDP-glucuronosyltransferase 1A8 shows functional localization to the basolateral plasma membrane. *J. Biol. Chem.* **2015**, *290* (12), 7622-7633.

(11) Radominska-Pandya, A.; Pokrovskaya, I. D.; Xu, J.; Little, J. M.; Jude, A. R.; Kurten, R. C.; Czernik, P. J. Nuclear UDP-glucuronosyltransferases: identification of UGT2B7 and UGT1A6 in human liver nuclear membranes. *Arch. Biochem. Biophys.* **2002**, *399* (1), 37-48.

(12) Maciejczyk, A.; Jagoda, E.; Wysocka, T.; Matkowski, R.; Gyorffy, B.; Lage, H.; Surowiak, P. ABCC2 (MRP2, cMOAT) localized in the nuclear envelope of breast carcinoma cells correlates with poor clinical outcome. *Pathol. Oncol. Res.* **2012**, *18* (2), 331-342.

(13) Dartier, J.; Lemaitre, E.; Chourpa, I.; Goupille, C.; Servais, S.; Chevalier, S.; Maheo, K.; Dumas, J. F. ATP-dependent activity and mitochondrial localization of drug efflux pumps in doxorubicin-resistant breast cancer cells. *Biochim. Biophys. Acta.* **2017**, *1861* (5 Pt A), 1075-1084.

(14) Bendayan, R.; Ronaldson, P. T.; Gingras, D.; Bendayan, M. In situ localization of P-glycoprotein (ABCB1) in human and rat brain. *J. Histochem. Cytochem.* **2006**, *54* (10), 1159-1167.

(15) Yamagishi, T.; Sahni, S.; Sharp, D. M.; Arvind, A.; Jansson, P. J.; Richardson, D. R. P-glycoprotein mediates drug resistance via a novel mechanism involving lysosomal sequestration. *J. Biol. Chem.* **2013**, *288* (44), 31761-31771.

(16) Zhang, J.; Zhou, F.; Lu, M.; Ji, W.; Niu, F.; Zha, W.; Wu, X.; Hao, H.; Wang, G. Pharmacokinetics-pharmacology disconnection of herbal medicines and its potential solutions with cellular pharmacokinetic-pharmacodynamic strategy. *Curr. Drug. Metab.* **2012**, *13* (5), 558-576. (17) Qin, Z.; Li, S.; Yao, Z.; Hong, X.; Wu, B.; Krausz, K. W.; Gonzalez, F. J.; Gao, H.; Yao, X. Chemical inhibition and stable knock-down of efflux transporters leads to reduced glucuronidation of wushanicaritin in UGT1A1-overexpressing HeLa cells: the role of breast cancer resistance protein (BCRP) and multidrug resistance-associated proteins (MRPs) in the excretion of glucuronides. *Food. Funct.* **2018**, *9* (3), 1410-1423.

(18) Zhang, X.; Dong, D.; Wang, H.; Ma, Z.; Wang, Y.; Wu, B. Stable knock-down of efflux transporters leads to reduced glucuronidation in UGT1A1-overexpressing HeLa cells: the evidence for glucuronidation-transport interplay. *Mol. Pharm.* **2015**, *12* (4), 1268-1278.

(19) Kong, L. L.; Shen, G. L.; Wang, Z. Y.; Zhuang, X. M.; Xiao, W. B.; Yuan, M.; Gong, Z. H.; Li, H. Inhibition of P-Glycoprotein and Multidrug Resistance-Associated Protein 2 Regulates the Hepatobiliary Excretion and Plasma Exposure of Thienorphine and Its Glucuronide Conjugate. *Front. Pharmacol.* **2016**, *7*, 242.

(20) Rajendran, P.; Rengarajan, T.; Nandakumar, N.; Palaniswami, R.; Nishigaki, Y.; Nishigaki, I. Kaempferol, a potential cytostatic and cure for inflammatory disorders. *Eur. J. Med. Chem.* **2014**, *86*, 103-112.

(21) Zeng, X.; Shi, J.; Zhao, M.; Chen, Q.; Wang, L.; Jiang, H.; Luo, F.; Zhu, L.; Lu, L.; Wang, X.et al. Regioselective Glucuronidation of Diosmetin and Chrysoeriol by the Interplay of Glucuronidation and Transport in UGT1A9-Overexpressing HeLa Cells. *PloS One* **2016**, *11* (11), e0166239.

(22) Mukai, R.; Shirai, Y.; Saito, N.; Yoshida, K.; Ashida, H. Subcellular localization of flavonol aglycone in hepatocytes visualized by confocal laser scanning fluorescence microscope. *Cytotechnology* **2009**, *59* (3), 177-182.

(23) Zheng, L.; Zhu, L.; Zhao, M.; Shi, J.; Li, Y.; Yu, J.; Jiang, H.; Wu, J.; Tong, Y.; Liu, Y.et al. In Vivo Exposure of Kaempferol Is Driven by Phase II Metabolic Enzymes and Efflux Transporters. *AAPS. J.* **2016**, *18* (5), 1289-1299.

(24) Hutzler, J. M.; Tracy, T. S. Atypical kinetic profiles in drug metabolism reactions. *Drug. Metab. Dispos.* **2002**, *30* (4), 355-362.

(25) Liu, X.; Tam, V. H.; Hu, M. Disposition of flavonoids via enteric recycling: determination of the UDP-glucuronosyltransferase isoforms responsible for the metabolism of flavonoids in intact Caco-2 TC7 cells using siRNA. *Mol. Pharm.* **2007**, *4* (6), 873-882.

(26) Singh, R.; Singh, B.; Singh, S.; Kumar, N.; Kumar, S.; Arora, S. Anti-free radical activities of kaempferol isolated from Acacia nilotica (L.) Willd. Ex. Del. *Toxicol. In vitro.* **2008**, *22* (8), 1965-1970.

(27) Soucek, P.; Kondrova, E.; Hermanek, J.; Stopka, P.; Boumendjel, A.; Ueng, Y. F.; Gut, I. New model system for testing effects of flavonoids on doxorubicin-related formation of hydroxyl radicals. *Anti-cancer Drugs* **2011**, *22* (2), 176-184.

(28) Gallorini, M.; Petzel, C.; Bolay, C.; Hiller, K. A.; Cataldi, A.; Buchalla, W.; Krifka, S.; Schweikl, H. Activation of the Nrf2-regulated antioxidant cell response inhibits HEMA-induced oxidative stress and supports cell viability. *Biomaterials* **2015**, *56*, 114-128.

(29) Duan, X.; Li, J.; Li, W.; Xing, X.; Zhang, Y.; Li, W.; Zhao, L.; Sun, G.; Gao, X. H.; Li, B. Antioxidant tert-butylhydroquinone ameliorates arsenic-induced intracellular damages and apoptosis through induction of Nrf2-dependent antioxidant responses as well as stabilization of anti-apoptotic factor Bcl-2 in human keratinocytes. *Free. Radic. Biol. Med.* **2016**, *94*, 74-87.

(30) Tang, L.; Li, Y.; Chen, W. Y.; Zeng, S.; Dong, L. N.; Peng, X. J.; Jiang, W.; Hu, M.; Liu, Z. Q. Breast cancer resistance protein-mediated efflux of luteolin glucuronides in HeLa cells overexpressing UDP-glucuronosyltransferase 1A9. *Pharm. Res*. **2014**, *31* (4), 847-860.

(31) Xia, B.; Zhou, Q.; Zheng, Z.; Ye, L.; Hu, M.; Liu, Z. A novel local recycling mechanism that enhances enteric bioavailability of flavonoids and prolongs their residence time in the gut. *Mol. Pharm.* **2012**, *9* (11), 3246-3258.

(32) Gao, S.; Hu, M. Bioavailability challenges associated with development of anti-cancer phenolics. *Mini. Rev. Med. Chem.* **2010**, *10* (6), 550-567.

(33) Barve, A.; Chen, C.; Hebbar, V.; Desiderio, J.; Saw, C. L.; Kong, A. N. Metabolism, oral bioavailability and pharmacokinetics of chemopreventive kaempferol in rats. *Biopharm. Drug. Dispos.* **2009**, *30* (7), 356-365.

(34) Zhang, J.; Zhou, F.; Wu, X.; Zhang, X.; Chen, Y.; Zha, B. S.; Niu, F.; Lu, M.; Hao, G.; Sun, Y.et al. Cellular pharmacokinetic mechanisms of adriamycin resistance and its modulation by 20(S)-ginsenoside Rh2 in MCF-7/Adr cells. *Br. J. Pharmacol.* **2012**, *165* (1), 120-134.

(35) Vadlapatla, R. K.; Vadlapudi, A. D.; Pal, D.; Mitra, A. K. Mechanisms of drug resistance in cancer chemotherapy: coordinated role and regulation of efflux

transporters and metabolizing enzymes. *Curr. Pharm. Des.* **2013**, *19* (40), 7126-7140.

(36) Rocha, M.; Hernandez-Mijares, A.; Garcia-Malpartida, K.; Banuls, C.; Bellod, L.; Victor, V. M. Mitochondria-targeted antioxidant peptides. *Curr. Pharm. Design.* **2010**, *16* (28), 3124-3131.

(37) Choi, E. M. Kaempferol protects MC3T3-E1 cells through antioxidant effect and regulation of mitochondrial function. *Food. Chem. Toxicol.* **2011**, *49* (8), 1800-1805.

(38) Feng, H.; Cao, J.; Zhang, G.; Wang, Y. Kaempferol Attenuates Cardiac Hypertrophy via Regulation of ASK1/MAPK Signaling Pathway and Oxidative Stress. *Planta. Med.* **2017**, *83* (10), 837-845.

(39) Silva, B.; Oliveira, P. J.; Dias, A.; Malva, J. O. Quercetin, kaempferol and biapigenin from Hypericum perforatum are neuroprotective against excitotoxic insults. *Neurotox. Res.* **2008**, *13* (3-4), 265-279.

(40) Zhou, M.; Ren, H.; Han, J.; Wang, W.; Zheng, Q.; Wang, D. Protective Effects of Kaempferol against Myocardial Ischemia/Reperfusion Injury in Isolated Rat Heart via Antioxidant Activity and Inhibition of Glycogen Synthase Kinase-3beta. *Oxid. Med. Cell. longev.* **2015**, *2015*, 481405.

(41) Laughney, A. M.; Kim, E.; Sprachman, M. M.; Miller, M. A.; Kohler, R. H.; Yang, K. S.; Orth, J. D.; Mitchison, T. J.; Weissleder, R. Single-cell pharmacokinetic imaging reveals a therapeutic strategy to overcome drug resistance to the microtubule inhibitor eribulin. *Sci. Transl. Med.* **2014**, *6* (261), 261ra152.

(42) Zhang, J.; Liu, D.; Zhang, M.; Sun, Y.; Zhang, X.; Guan, G.; Zhao, X.; Qiao, M.; Chen, D.; Hu, H. The cellular uptake mechanism, intracellular transportation, and exocytosis of polyamidoamine dendrimers in multidrug-resistant breast cancer cells. *Int. J. Nanomedicine.* **2016**, *11*, 3677-3690.

(43) Yuan, Z. W.; Leung, E. L.; Fan, X. X.; Zhou, H.; Ma, W. Z.; Liu, L.; Xie, Y. Quantitative evaluation of berberine subcellular distribution and cellular accumulation in non-small cell lung cancer cells by UPLC-MS/MS. *Talanta*

2015, *144*, 20-28.

Figure Captions

Figure 1. The *in vitro* glucuronidation characteristics of kaempferol. The final protein concentrations were 0.0106-0.2 $mg \cdot mL^{-1}$, and the reaction time was 20 min based on optimization of the reaction. (A and B) Glucuronidation rates of kaempferol by 12 recombinant human UGTs were determined at three substrate concentrations (1.25, 2.5 and 10 μM). (C-H) Enzyme kinetics of kaempferol in UGT1A9, HIMs and HLMs were determined at serial concentrations of kaempferol (0.125-40 μM). Curves were estimated based on fitted parameters generated by the Michaelis-Menten (C and D) or Biphasic equation (E-H), and the Eadie-Hofstee plots are shown in the inset, respectively. Values are mean ± SD (n = 3).

Figure 2. UGT1A9 and efflux transporter inhibitors promoted the accumulation of kaempferol in subcellular organelles. Cells were incubated with 50 μM kaempferol in the absence or presence of chemical inhibitors for 5, 15, 30, 45, and 60 min. Then nuclei, mitochondria (Mito), endoplasmic reticulum (ER), and lysosome were stained with various organelle-specific fluorescent dyes. Confocal images were collected using a LSCM. The green fluorescence indicates kaempferol. Blue denotes nuclei. Red shows mitochondria, endoplasmic reticulum and lysosome, respectively. Yellow indicates overlay of green signal with red signal. (A-D) The accumulation of kaempferol in the nuclei, mitochondria, endoplasmic reticulum and lysosome, respectively. (a-d) Fluorescence quantification of kaempferol are presented as mean ± SD (n = 3). See also Figures S1-S4.

Figure 3. Efflux transporters control the subcellular glucuronidation rates of kaempferol. Cells were incubated with 20 μM kaempferol in the absence or presence of UGT1A9 and efflux transporter inhibitors for 5, 15, 30, 45, and 60 min. The subcellular fractions were then extracted, and the concentrations of kaempferol and its glucuronides were quantified by UHPLC-MS/MS. Triplicate samples used for detection and each data point represent the mean ± SD. (A-E) Kaempferol; (F-J) K-3-G; (K-O) K-7-G.

Figure 4. Correlation between fluorescence density and absolute amounts of kaempferol in subcellular organelles. r^2 indicates Pearson correlation coefficient. (A) Nuclei; (B) Mitochondria; (C) Endoplasmic reticulum; (D) Lysosome.

Figure 5. Knockout of efflux transporter significantly increased the subcellular

accumulation of kaempferol in liver and intestine. After oral administration of 100 $mg \cdot kg^{-1}$ kaempferol for 30 min, the liver and jejunum were rapidly removed and cut into 4-μm sections. The nuclei (blue) and mitochondria (red) of tissues were then stained and observed with a LSCM. (A) Liver; (B) Jejunum; (C) Values indicate mean fluorescence densities of kaempferol ± SD (n = 4). Independent-samples T test was used for data analysis. $^{*}P < 0.05$ compared with liver of wild-type mice; $^{\#}P < 0.05$ compared with jejunum of wild-type mice.

Figure 6. Kaempferol suppressed intracellular ROS formation in a dose-dependent manner. Cells were incubated with kaempferol (20 and 50 μM) in the absence or presence of chemical inhibitors for 30 min. Control group was treated with blank HBSS. N-acetyl-L-cysteine (NAC) was used as a positive control. Intracellular ROS was then labelled with CellROX® Orange Reagent, and nuclei were stained with Hoechst 33342. Images were acquired with a LSCM. (A) Fluorescent images; (B) Mean fluorescence densities of ROS ± SD (n = 3). Independent-samples T test was used for data analysis. The asterisk (*) indicates statistically significant differences ($P < 0.05$).

Figure 7. Kaempferol induced the expression and nuclear translocation of Nrf2 in a dose-dependent manner. Cells were incubated with kaempferol (20 and 50 μM) in the absence or presence of chemical inhibitors for 30 min. The control group was treated with blank HBSS. NAC was used as a positive control. Cells were then fixed with 4% formaldehyde and immunostained with anti-Nrf2 antibody (shown in red). Nuclei were labelled in blue with DAPI. The image was obtained with a LSCM. (A) Immunofluorescence image; (B) Mean fluorescence densities of Nrf2 ± SD (n = 3). Independent-samples T test was used for data analysis. The asterisk (*) indicates statistically significant differences ($P < 0.05$).

Figure 1

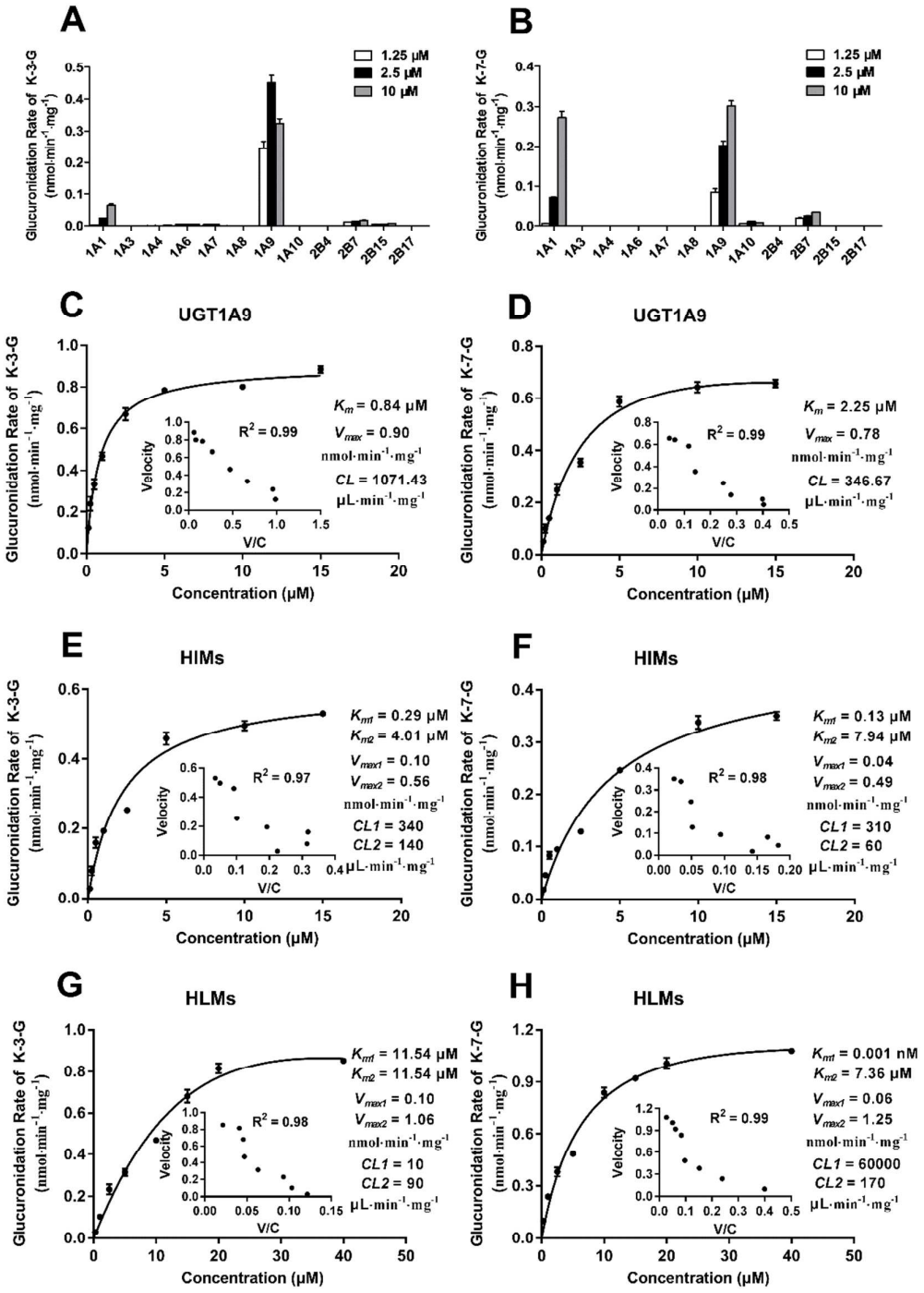
A
1.25 μM
2.5 μM
10 μM
Glucuronidation Rate of K-3-G (nmol·min⁻¹·mg⁻¹)
1A1 1A3 1A4 1A6 1A7 1A8 1A9 1A10 2B4 2B7 2B15 2B17
B
1.25 μM
2.5 μM
10 μM
Glucuronidation Rate of K-7-G (nmol·min⁻¹·mg⁻¹)
1A1 1A3 1A4 1A6 1A7 1A8 1A9 1A10 2B4 2B7 2B15 2B17
C
UGT1A9
Glucuronidation Rate of K-3-G (nmol·min⁻¹·mg⁻¹)
Km = 0.84 μM
Vmax = 0.90 nmol·min⁻¹·mg⁻¹
CL = 1071.43 μL·min⁻¹·mg⁻¹
R² = 0.99
Velocity
V/C
Concentration (μM)
D
UGT1A9
Glucuronidation Rate of K-7-G (nmol·min⁻¹·mg⁻¹)
Km = 2.25 μM
Vmax = 0.78 nmol·min⁻¹·mg⁻¹
CL = 346.67 μL·min⁻¹·mg⁻¹
R² = 0.99
Velocity
V/C
Concentration (μM)
E
HIMs
Glucuronidation Rate of K-3-G (nmol·min⁻¹·mg⁻¹)
Km1 = 0.29 μM
Km2 = 4.01 μM
Vmax1 = 0.10
Vmax2 = 0.56 nmol·min⁻¹·mg⁻¹
CL1 = 340
CL2 = 140 μL·min⁻¹·mg⁻¹
R² = 0.97
Velocity
V/C
Concentration (μM)
F
HIMs
Glucuronidation Rate of K-7-G (nmol·min⁻¹·mg⁻¹)
Km1 = 0.13 μM
Km2 = 7.94 μM
Vmax1 = 0.04
Vmax2 = 0.49 nmol·min⁻¹·mg⁻¹
CL1 = 310
CL2 = 60 μL·min⁻¹·mg⁻¹
R² = 0.98
Velocity
V/C
Concentration (μM)
G
HLMs
Glucuronidation Rate of K-3-G (nmol·min⁻¹·mg⁻¹)
Km1 = 11.54 μM
Km2 = 11.54 μM
Vmax1 = 0.10
Vmax2 = 1.06 nmol·min⁻¹·mg⁻¹
CL1 = 10
CL2 = 90 μL·min⁻¹·mg⁻¹
R² = 0.98
Velocity
V/C
Concentration (μM)
H
HLMs
Glucuronidation Rate of K-7-G (nmol·min⁻¹·mg⁻¹)
Km1 = 0.001 nM
Km2 = 7.36 μM
Vmax1 = 0.06
Vmax2 = 1.25 nmol·min⁻¹·mg⁻¹
CL1 = 60000
CL2 = 170 μL·min⁻¹·mg⁻¹
R² = 0.99
Velocity
V/C
Concentration (μM)

Figure 2

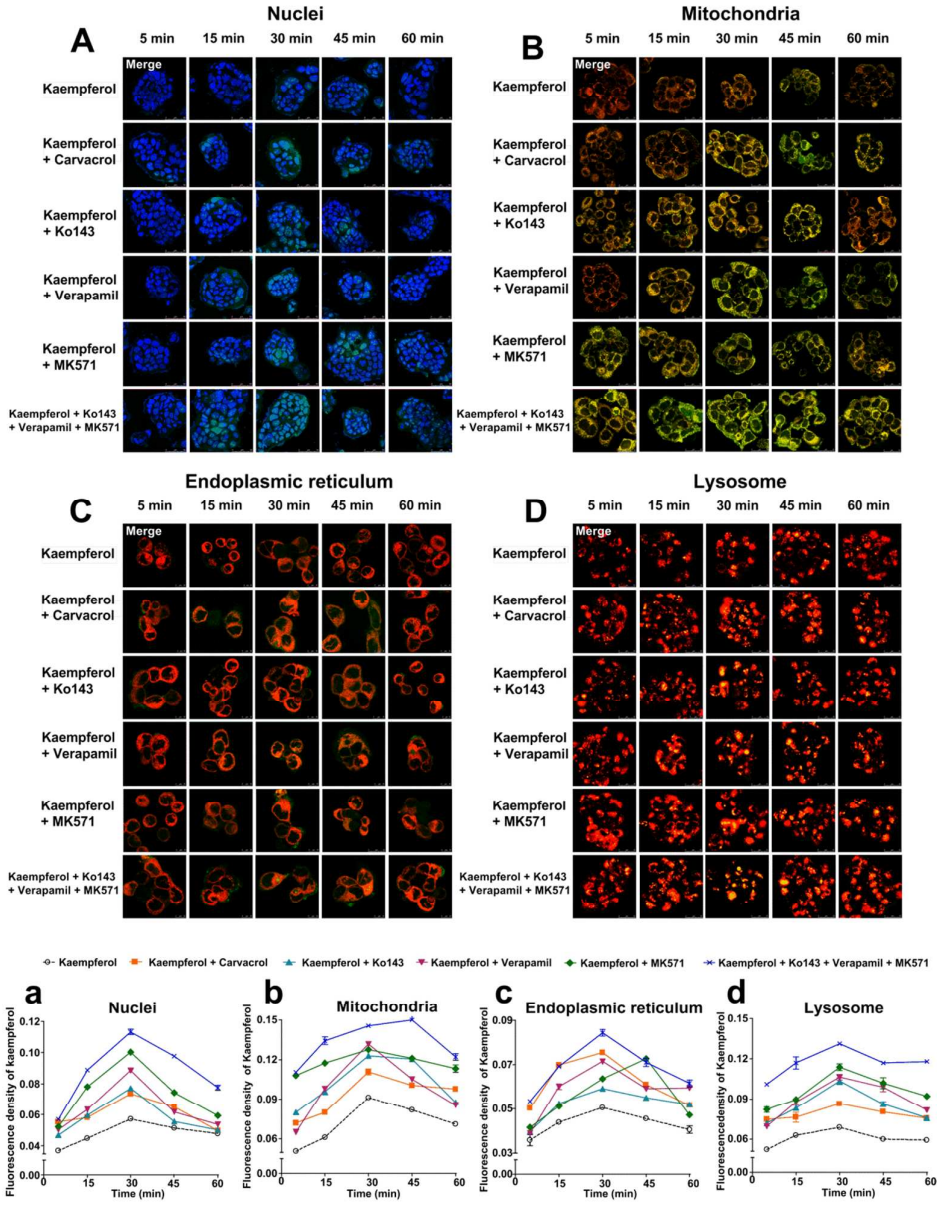
Nuclei
Mitochondria
Endoplasmic reticulum
Lysosome
A
B
C
D
5 min
15 min
30 min
45 min
60 min
Merge
Kaempferol
Kaempferol + Carvacrol
Kaempferol + Ko143
Kaempferol + Verapamil
Kaempferol + MK571
Kaempferol + Ko143 + Verapamil + MK571
a
b
c
d
Fluorescence density of kaempferol
Time (min)

Figure 3

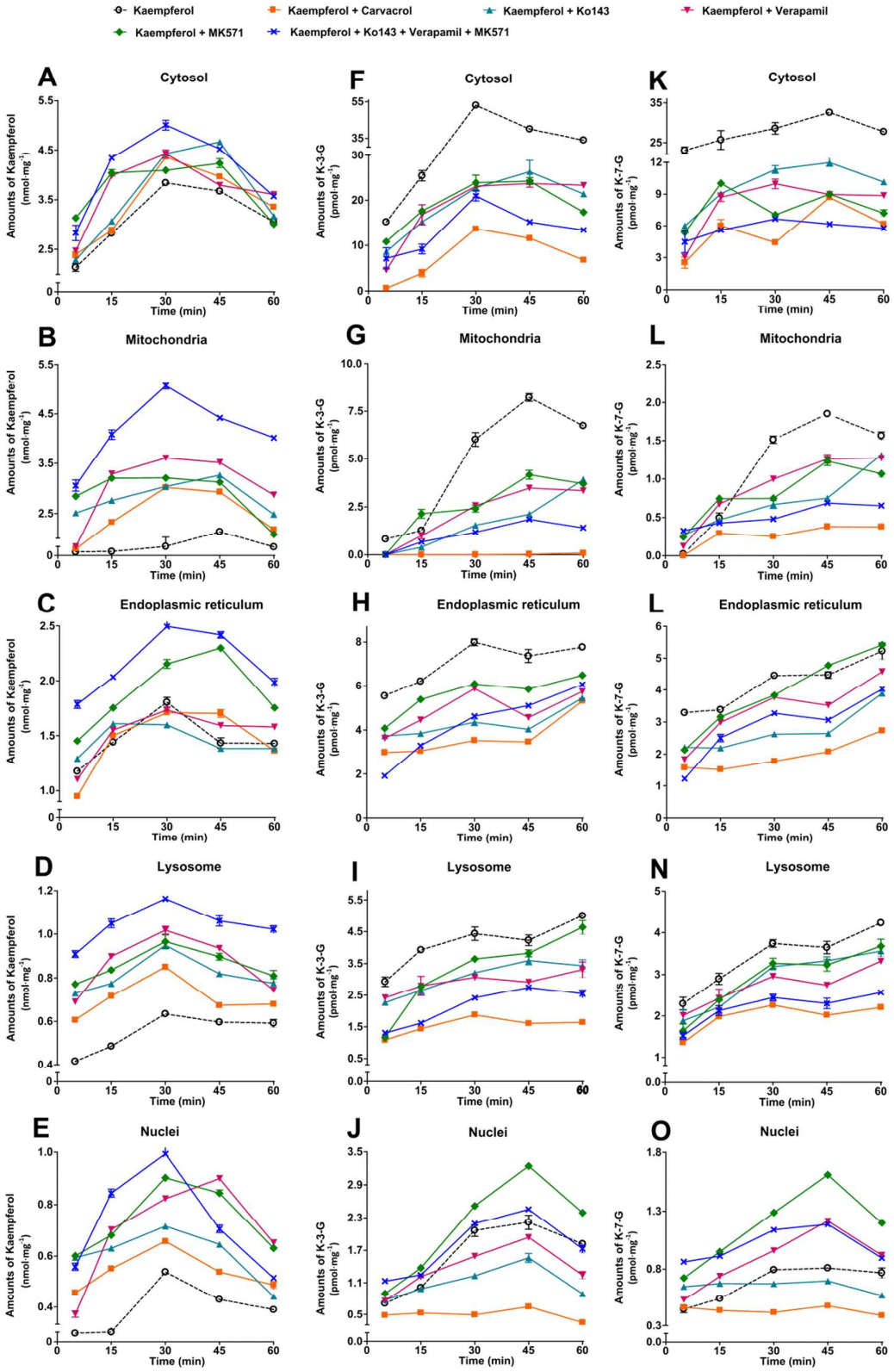
Kaempferol
Kaempferol + Carvacrol
Kaempferol + Ko143
Kaempferol + Verapamil
Kaempferol + MK571
Kaempferol + Ko143 + Verapamil + MK571
A
Cytosol
Amounts of Kaempferol (nmol·mg-1)
F
Cytosol
Amounts of K-3-G (pmol·mg-1)
K
Cytosol
Amounts of K-7-G (pmol·mg-1)
B
Mitochondria
G
Mitochondria
L
Mitochondria
C
Endoplasmic reticulum
H
Endoplasmic reticulum
L
Endoplasmic reticulum
D
Lysosome
I
Lysosome
N
Lysosome
E
Nuclei
J
Nuclei
O
Nuclei
Time (min)

Figure 4

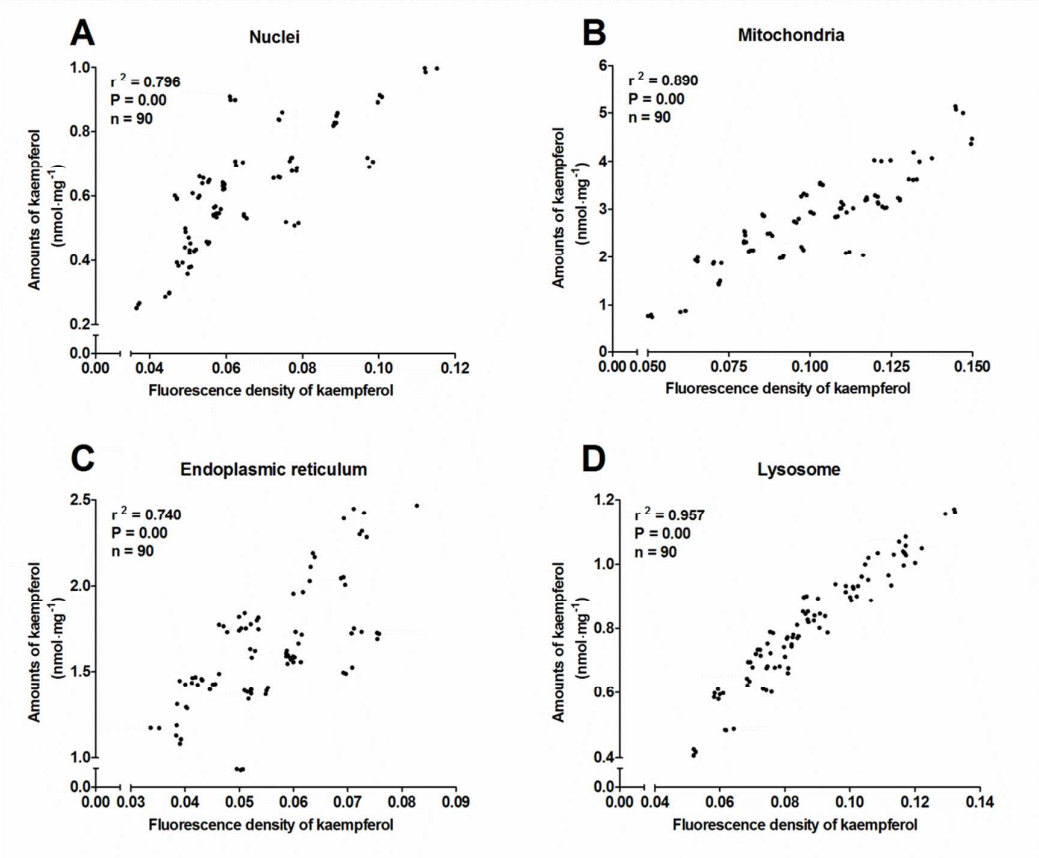
A
Nuclei
r 2 = 0.796
P = 0.00
n = 90
Amounts of kaempferol (nmol·mg-1)
Fluorescence density of kaempferol
B
Mitochondria
r 2 = 0.890
P = 0.00
n = 90
Amounts of kaempferol (nmol·mg-1)
Fluorescence density of kaempferol
C
Endoplasmic reticulum
r 2 = 0.740
P = 0.00
n = 90
Amounts of kaempferol (nmol·mg-1)
Fluorescence density of kaempferol
D
Lysosome
r 2 = 0.957
P = 0.00
n = 90
Amounts of kaempferol (nmol·mg-1)
Fluorescence density of kaempferol

Figure 5

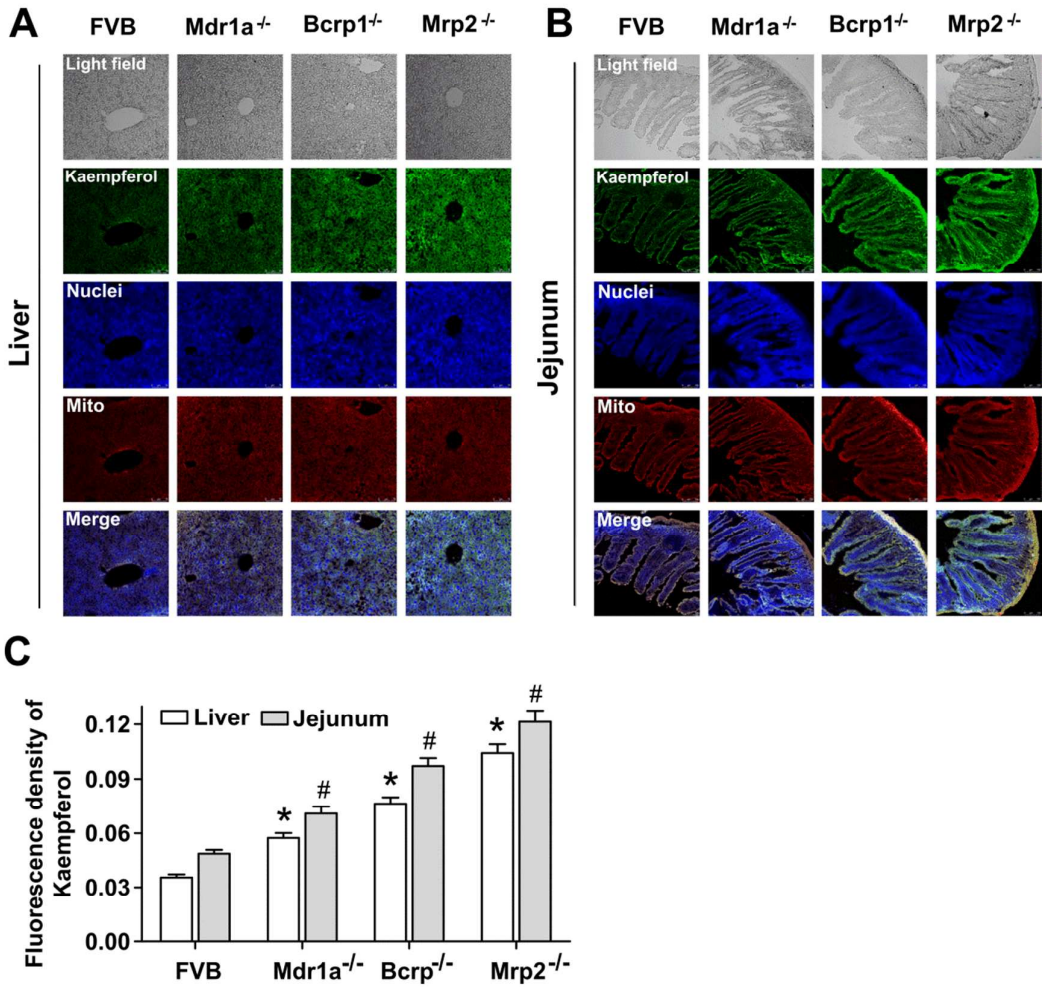
A
FVB
Mdr1a-/-
Bcrp1-/-
Mrp2-/-
Light field
Kaempferol
Nuclei
Mito
Merge
Liver
B
FVB
Mdr1a-/-
Bcrp1-/-
Mrp2-/-
Light field
Kaempferol
Nuclei
Mito
Merge
Jejunum
C
Fluorescence density of Kaempferol
0.12
0.09
0.06
0.03
0.00
Liver
Jejunum
*
#
*
#
*
#
FVB
Mdr1a-/-
Bcrp-/-
Mrp2-/-

Figure 6

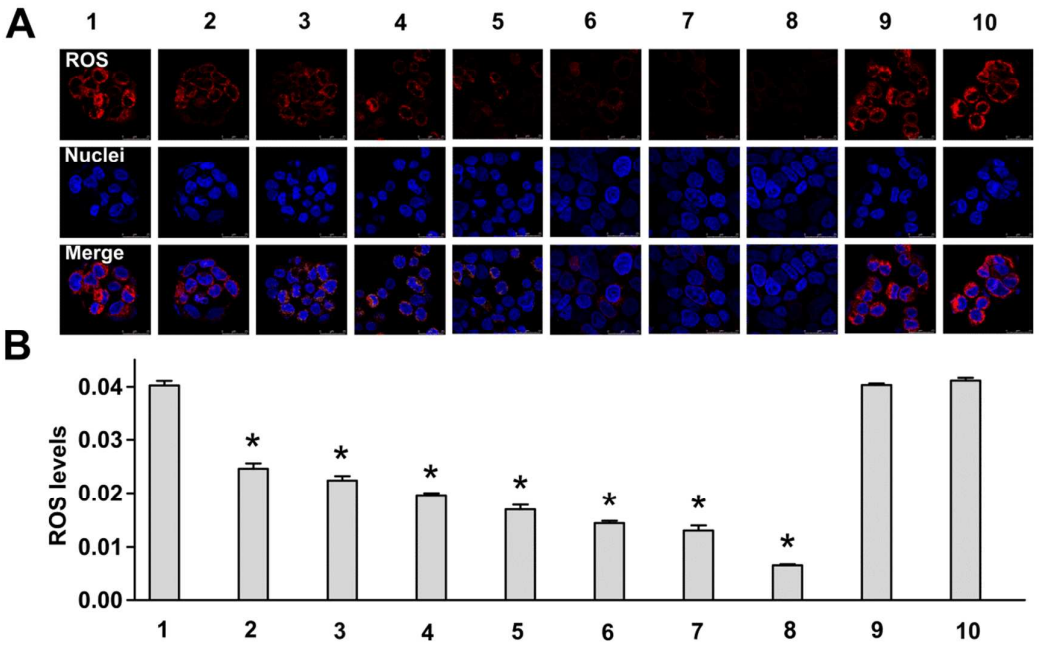

(1) Control; (2) NAC; (3) 20 μM Kaempferol; (4) 20 μM Kaempferol + Carvacrol; (5) 20 μM Kaempferol + Ko143 + Verapamil + MK571; (6) 50 μM Kaempferol; (7) 50 μM Kaempferol + Carvacrol; (8) 50 μM Kaempferol + Ko143 +Verapamil + MK571; (9) Carvacrol; (10) Ko143 +Verapamil + MK571.

Figure 7

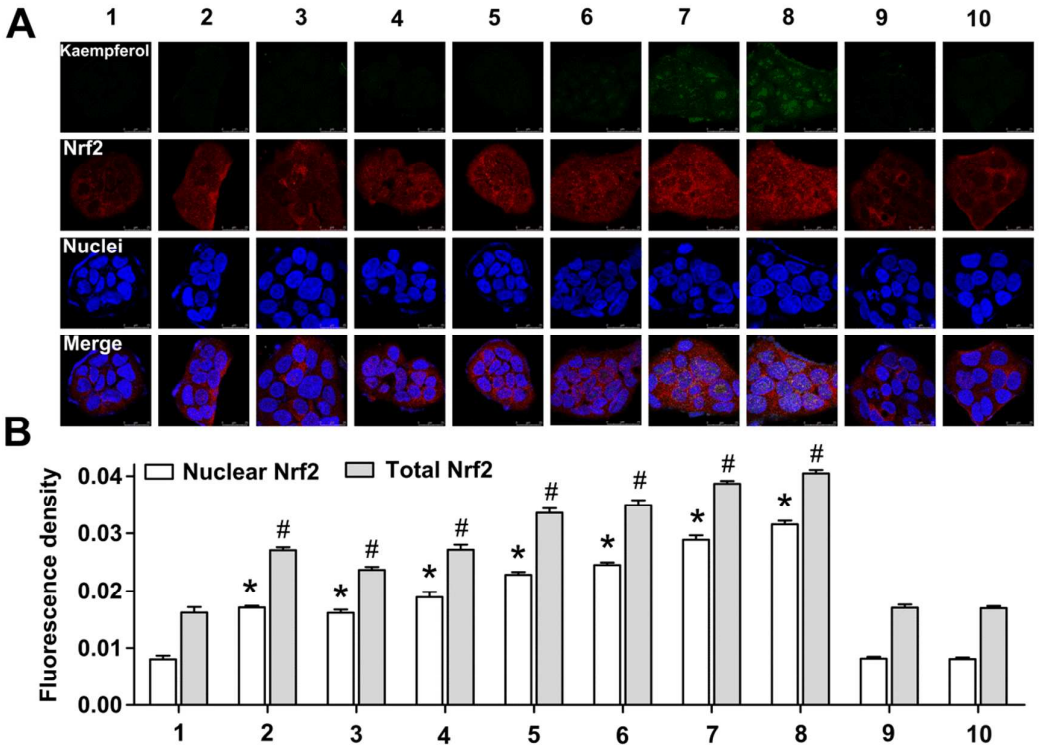

(1) Control; (2) NAC; (3) 20 μM Kaempferol; (4) 20 μM Kaempferol + Carvacrol; (5) 20 μM Kaempferol + Ko143 + Verapamil + MK571; (6) 50 μM Kaempferol; (7) 50 μM Kaempferol + Carvacrol; (8) 50 μM Kaempferol + Ko143 +Verapamil + MK571; (9) Carvacrol; (10) Ko143 +Verapamil + MK571.

Supporting Information

Effect of UGT1A9 and efflux transporter inhibitors on subcellular accumulation of kaempferol; MRM chromatograms; influence of efflux transporters on the subcellular glucuronidation of kaempferol; dynamic distribution of the subcellular kaempferol and its glucuronides in Caco-2/TC7 cell; time-lapse analysis of kaempferol accumulation in subcellular organelles; the hydrolysis of kaempferol glucuronides in Caco-2/TC7 cell lysates

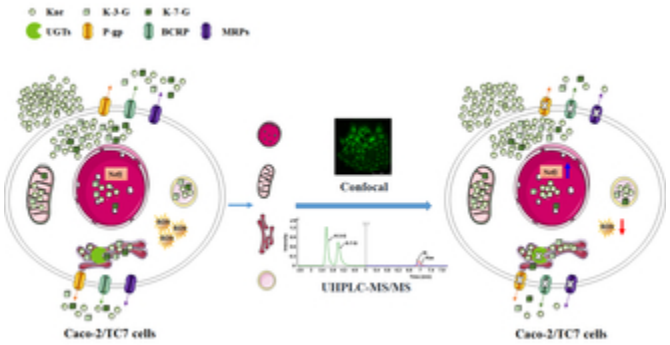

28x14mm (300 x 300 DPI)